Comparisons of Rain Estimates from Ground Radar And Satellite Over Mountainous Regions

Xin Lin*, Chris Kidd*, Jing Tao[+], and Ana Barros[+]

For submission to ***The Journal of Hydrometeorology***

Corresponding author address:

Dr. Xin Lin,
Atmospheric Mesoscale Processes Branch,
NASA Goddard Space Flight Center, Code 612,
Greenbelt, MD 20771.

Tel: 443-370-6792
E-mail: xlin.lin-1@nasa.gov

* Additional Affiliation: ESSIC, University of Maryland, College Park, College Park, Maryland.
[+] Affiliation: Civil and Environmental Engineering Department, Pratt School of Engineering, Duke University, Durham, North Carolina.

Abstract

A high-resolution rainfall product merging surface radar and an enhanced gauge network is used as a reference to examine two operational surface radar rainfall products over mountain areas. The two operational rainfall products include radar-only and conventional-gauge-corrected radar rainfall products. Statistics of rain occurrence and rain amount including their geographical, seasonal, and diurnal variations are examined using 3-year data. It is found that the three surface radar rainfall products in general agree well with one another over mountainous regions in terms of horizontal mean distributions of rain occurrence and rain amount. Frequency of rain occurrence and fraction of rain amount also indicate similar distribution patterns as a function of rain intensity. The diurnal signals of precipitation over mountain ridges are well captured and joint distributions of coincident raining samples indicate reasonable correlations during both summer and winter.

Factors including undetected low-level precipitation, limited availability of gauges for correcting the Z-R relationship over the mountains, and radar beam blocking by mountains are clearly noticed in the two conventional radar rainfall products. Both radar-only and conventional-gauge-corrected radar rainfall products underestimate the rain occurrence and fraction of rain amount at intermediate and heavy rain intensities. Comparison of PR and TMI against a surface radar-only rainfall product indicates that the PR performs equally well with the high-resolution radar-only rainfall product over complex terrains at intermediate and heavy rain intensities during the summer and winter. TMI, on the other hand, requires improvement to retrieve wintertime precipitation over mountain areas.

1. Introduction

Rainfall estimates over mountainous regions are known to have large uncertainties due to highly variable and complicated precipitation features associated with topography (e.g., Barros et al. 2000; Prat and Barros 2010; Yamamoto et al. 2011). As one of the main ground-based rainfall-measuring instruments over land, rain gauges are not only sparse over remote mountainous regions, but also suffer from calibration and representativeness errors. Ground radars can provide continual rain retrievals covering large areas, but their rainfall estimates may have large biases due to factors such as undetected low-level precipitation under the lowest radar beam elevation often caused by radar beam blocking by mountains. In addition, the lack of well-calibrated rain gauge data also severely limits bias corrections of the ground radar rainfall over mountainous regions. Therefore, the commonly-used surface rainfall reference data from conventional gauge and ground radar network have issues over mountainous regions and should be used with great care.

Satellite observations have been widely utilized to extract instantaneous estimates of rainfall information on the global scale, and provide a promising way to capture precipitation characteristics over mountainous regions at fine temporal and spatial resolutions. Among various remote-sensing instruments, microwave sensors that directly respond to the absorption and scattering of cloud hydrometeor particles are the backbone of space-based precipitation measurements. For example, the precipitation radar (PR) (Meneghini and Kozu 1990; Kummerow et al 1998; Iguchi et al. 2000; Kummerow et al. 2000) on board the Tropical Rainfall Measuring Mission (TRMM, Simpson et al. 1988, 1996) satellite provided the first space-borne rainfall retrievals from an active microwave

sensor. The recently-launched Dual-frequency Precipitation Radar (DPR) on board the Global Precipitation Measuring mission (GPM, Hou et al. 2014) core satellite has additional capabilities for measuring light rain and falling snow. Considering PR and DPR's active microwave sensing features, these radar data may serve as space-borne rain references for assessing other satellite rainfall retrievals and even surface measurements. In addition to the space-borne precipitation radars, passive microwave (PMW) radiometers and sounders, featuring wider ground track coverage, have been widely utilized to retrieve surface rainfall over land using high-frequency scattering-based algorithms.

Due to the sensitivity and spatial resolution of satellite instruments and retrieval algorithms, satellite rainfall products also have problems over mountainous regions due to topography and partial beam filling. For PMW retrievals, the highly variable land surface with different vegetation, snow and ice, and soil moisture (which may also change significantly with time) makes it difficult to distinguish rainfall against the complicated surface background (e.g., Wilheit 1986; Kummerow et al. 2000; Ferraro et al, 2005).

A major obstacle in assessing rainfall estimates over mountainous regions is due to the large uncertainties that surface measurements and satellite retrievals have at fine temporal and spatial scales: there are no perfect observations to serve as the “truth”. The National Mosaic and Multi-sensor QPE (NMQ, QPE: quantitative precipitation estimates) project at the National Oceanic and Atmospheric Administration (NOAA) National Severe Storms Laboratory (NSSL) provides a number of experimental QPE products operationally. These QPE products, including radar-only and gauge-corrected radar

106 rainfall estimates originally derived from about 140 WSR-88D operational radar with
107 updated rain-reflectivity algorithms, cover the entire continental US at high spatial
108 resolution (0.01º×0.01º) (Vasiloff et al. 2007; Zhang et al. 2011). These surface rainfall
109 products have provided many valuable insights on weather analyses and severe storm
110 forecasts over the continental US as well as providing a basis for satellite rain error
111 estimates over land. Noting the uncertainty in gauge-corrected radar rainfall estimates
112 over complex terrains, Tao and Barros (2013) further adjusted the hourly gauge-corrected
113 radar rainfall product using the very dense rain gauge observations in the Pigeon River
114 basin in the Southern Appalachian Mountains.

115 In this study, we use a similar gauge-enhanced high-resolution radar rainfall product
116 as the reference to evaluate two operational surface radar and gauge-radar merged rainfall
117 products (radar only and conventional gauge-adjusted). With a better understanding of
118 the statistical characteristics including the strength and weakness of these radar rainfall
119 products, satellite rainfall retrievals from both active and passive microwave sensors
120 onboard the TRMM satellite, TRMM PR and TRMM Microwave Imager (TMI), are also
121 coincidently examined against a 5-minute radar-only rainfall product over mountainous
122 regions. Specifically, we intend to 1) quantitatively examine the rain detection and
123 statistics as a function of rain intensity in different seasons over the mountains; 2) discuss
124 strengths and limitations of ground-based radar-only and radar-gauge merged products in
125 estimating rain occurrence and rain accumulation; 3) evaluate to what extent the current
126 space-borne precipitation radar could help to improve rainfall estimates in mountainous
127 regions. Section 2 introduces the dataset and analysis methodologies while Section 3
128 evaluates surface radar rainfall products against the reference dataset over the

129 mountainous region. Section 4 compares coincident satellite rainfall retrievals from
130 TRMM PR and TMI against surface radar rainfall estimates. Finally, the conclusions of
131 the study are presented in Section 5.

132

133 2. Data and Analysis Methods

134 *2.1 The surface radar rainfall product*

135 The NOAA NSSL, along with university research communities, provide two
136 experimental Next Generation Multi-sensor QPE (Q2) hourly products covering the
137 entire US continent at high spatial resolutions ($0.01^o \times 0.01^o$) (Vasiloff et al. 2007; Zhang
138 et al. 2011): the WSR-88D radar-only-based rainfall product (Q2rad) and the
139 conventional-gauge-corrected radar rainfall product (Q2rad_GC). Q2rad_GC is generated
140 by applying radar-gauge bias fields calculated using hourly rain gauge observations to
141 hourly Q2rad: comparisons show that Q2rad_GC in general performs better than Q2rad
142 (Ware 2005; Zhang et al. 2011). However, it was also found that Q2rad_GC still
143 underestimated rainfall significantly over the complex terrain of the Pigeon River basin in
144 the Southern Appalachian Mountains (Tao and Barros 2013). Chen et al. (2014)
145 compared Q2 products with gauge analysis and other rainfall products and also noticed
146 large uncertainties over mountain regions. Thus, the hourly Q2rad_GC product was
147 further adjusted by Tao and Barros (2013) in the Pigeon River basin in the Southern
148 Appalachian Mountains using the very dense rain gauge observations.

149 Figure 1 shows the conventional WSR-88D radar sites covering the Pigeon River
150 basin. The two ground radar sites (KMRX in Knoxville/Tennessee and KGSP in

151 Greer/South Carolina) lie in within 100 km of the Pigeon River basin, and at least 50 km
152 either side of the Southern Appalachian Mountains. Note the boundary of the basin is
153 coincident with the ridge lines, which causes the basin a land-lock region (blind-zone) for
154 the ground radars, implying that the rainfall spatial variability associated with orographic
155 modulation within the basin can hardly captured by the ground radars. Figure 2 details
156 the topography of the Pigeon River basin, located in Haywood County, North Carolina,
157 and the locations of rain gauges available from three different sources. There is 1 rain
158 gauge from the Environment and Climate Observing Network (ECONet) and 5 rain
159 gauges from Hydrometeorology Automated Data System (HADS). Both the ECONet and
160 HADS gauges are installed at low elevations or in valleys. It should be noted that the
161 HADS precipitation datasets are one of the major sources of rain gauge observations used
162 operationally to derive the multi-sensor QPE fields and adjust the Q2 product (Kim et al.
163 2009; Nelson et al. 2010; Seo 1998; Seo and Breidenbach 2002). The local-adjustment
164 for the Q2 (Q2rad) product at NSSL to produce the gauge-corrected Q2 (Q2rad_GC)
165 does not however always use all the HADS records probably due to data latency.
166 Considering that the locations of, and observations from conventional gauges used in
167 Q2rad_GC are very limited, as well as factors such as radar beam-blocking and beam
168 over-shooting, it is clear why considerable uncertainties still remain in the conventional-
169 gauge-corrected Q2 product over the mountainous region.

170 Tao and Barros (2013) developed two simple methods based on linear regression to
171 enhance the hourly gauge-corrected Q2rad_GC by incorporating high-quality-controlled
172 rainfall dataset from the Great Smoky Mountains Rain Gauge Network (GSMRGN, also
173 a 1st phase of the Precipitation Measuring Mission rain gauge network). GSMRGN has

35 tipping bucket gauges which are installed at mid to high elevations along exposed ridges in the Southern Appalachians; 32 gauges are within the Pigeon River Basin (see Figure 2). Further study by Wilson and Barros (2014) indicated that in mountainous regions of moderate topography and humid climate such as the Appalachians, light rainfall could explain accounts for a significant fraction of the annual precipitation (up to 50% on average in the Appalachians) and exhibited persistent spatial and seasonal patterns. Consequently, a new bias-correction method was developed to solve the problem of nonlinearity between the rainfall estimates and gauge observations that is largely attributed to the different rainfall-intensity regimes. This new method utilizes the probability density function (PDF) and cumulative distribution function (CDF) of areal rainfall fields interpolated from rain gauge observations using IDW (Inverse Distance Weighting) method, to divide the whole study domain into a heavy rainfall domain and a non-heavy rainfall domain. Specifically, the empirical PDF and CDF are calculated first, and then the quantile of 0.9 ($CDF_{0.9}$) is estimated based on the CDF curve, which is used as a threshold for separating the region, i.e. the region with the rainfall above $CDF_{0.9}$ is the heavy rainfall domain, while the region that below $CDF_{0.9}$ is the moderate or light rainfall domain. Then, linear regression between rainfall estimates and gauge observations is applied separately in each domain, and the derived regression coefficients are retrospectively applied to each domain to adjust Q2rad_GC in the same manner as in Tao and Barros (2013), in such a way that the nonlinearity is resolved by separating the rainfall regimes. The new adjusting methods is used to adjust Q2rad_GC data (Jun. 2008 – Oct. 2011) in the Pigeon River Basin along with the methods discussed by Tao and Barros (2013). The computed RMSEs (Table 1) show that the Q2+_cdfThr generated by

this new CDF threshold-based method which resolves the nonlinearity between the Q2rad_GC data and rain gauge observations, has the lowest overall RMSE, outperforming all the other products. In this study, we therefore use this special gauge-enhanced Q2 rainfall product adjusted by the CDF threshold over the Pigeon River basin as the reference to evaluate the other two Q2 rainfall products (Q2rad and Q2rad_GC). For simplicity, we will call this new Q2 rainfall product as Q2+ in the following sections.

2.2 Satellite rainfall retrievals

Past studies evaluating satellite rainfall retrievals were usually conducted at relatively large temporal and spatial resolutions. In recent years, more and more emphasis effort has been placed on hydrologic applications at finer scale with mesoscale precipitating systems. Because the selected mountain area with the high-resolution gauge network is relatively small (66 km x 61 km) and because the widths of ridges and valleys are usually narrow, it is difficult to distinguish mountain ridges and valleys using retrievals with large footprint sizes. We therefore in this study only examine satellite rainfall retrievals from TRMM PR and TMI (the level-2 products: 2A25 and 2A12)

The TRMM satellite was launched in November 1997 to improve our understanding of the temporal and spatial distributions of precipitation and latent heating in the Tropics and subtropics (Simpson et al. 1988; Kummerow et al. 1998). TRMM's orbit is circular, with an inclination angle of 35° relative to the Equator. PR and TMI are two microwave sensors onboard TRMM to retrieve precipitation and latent heat: the TMI is a 9-channel passive microwave radiometer measuring radiances at five frequencies, while the PR is the first quantitative space-borne *Ku*-band weather radar. Due to their differences in swath (TMI: 878 km; PR: 247 km, boosted after August 2001), the TMI samples a given

220 area over the Tropics and subtropics about once per day, but at a different local time
221 every day, while PR visits a given area on the average of about once every 3 days.

222 As described in Iguchi et al. (2000), the PR algorithm utilizes a globally averaged
223 drop-size distribution (DSD) as the initial guess to obtain attenuation-corrected radar
224 reflectivity-rain rate (*Ze*-R) relationship that is consistent with the assumed DSD model:
225 After taking into attenuation correction, the true effective reflectivity factor *Ze* is first
226 estimated at 13.8 GHz at each radar resolution cell from the measured vertical profiles of
227 reflectivity factor. The rainfall rate R is then computed from the estimated *Ze*. Several
228 factors, as discussed by Iguchi et al. (2000) and Masunaga et al (2002), may affect the
229 accuracy of the estimated rain rate: (1) assumptions in the DSD model; (2) uncertainties
230 in the attenuation correction; (3) corrections for non-uniform beam-filling effects. The
231 footprint resolution of a PR rain pixel is about 5 km at nadir and the minimum detectable
232 rain rate is about 0.3-0.5 mm h^{-1}.

233 The microwave rainfall retrievals used for TMI and many other imagers are
234 essentially based on the most recent version of the NASA Goddard Profiling (GPROF
235 version 7) algorithm (Kummerow et al. 1998; Olson et al. 1999; Kummerow et al. 2001;
236 Olson et al 2006; Masunaga and Kummerow 2005; Kummerow et al. 2011). Over land,
237 passive microwave sensors can measure the scattering effects of ice particles that later
238 melt to form raindrops. Cloud ice water content is first retrieved (Zhao and Weng 2002;
239 Weng et al. 2003) and surface rainfall is estimated based on empirical regressions
240 established to match PR rainfall (Ferraro et al. 1998, 2000, 2005; Kummerow et al.
241 2011). The footprint resolution of a TMI rain pixel is about 5.1 km at 85.5 GHz and the
242 minimum detectable rain rate is about 1.0 mm h^{-1} in the GPROF algorithm.

243 *2.3 Analysis methods*

244 One of the main objectives of this study is to evaluate two experimental surface radar
245 rainfall products over the mountainous region. Surface radar hourly rainfall products
246 including the radar-only Q2 (Q2rad) and gauge-corrected Q2 (Q2rad_GC) are compared
247 with the gauge-enhanced Q2+ data for the period from 1 January 2009 through 31
248 October 2011 over the Pigeon River basin (83.31ºW to 82.66ºW, 35.24ºN to 35.84ºN).
249 The evaluation of surface radar rainfall products in terms of rain accumulation, frequency
250 of rain occurrence and fraction of rain amount are conducted at their original temporal
251 and spatial resolutions (0.01º x 0.01º, 1-h intervals).

252 Because mountain ridges and valleys usually have distinctly different diurnal
253 variations of precipitation, the Shuttle Radar Topography Mission (SRTM) 0.01ºx0.01º
254 elevation data (derived from US Geography Survey's SRTM30) are used to divide the
255 mountain area into ridges and valleys. The grid points where SRTM elevation data are
256 higher than 1200 m are defined as the ridge area, while the grid points along the Pigeon
257 River where SRTM elevation data are lower than 1000 m are defined as the valley area. It
258 should be noted that the ridge area as defined by the elevation data are mainly over the
259 west side of Pigeon River Basin where most GSMRGN rain gauges are located.

260 Instantaneous satellite rainfall estimates can only be coincidently compared against
261 the gauge-corrected hourly surface radar data when the characteristics of rain events do
262 not change much within an hour. Precipitation, however, can be highly variable over
263 mountainous regions, particularly for those transient rain events which could develop and
264 dissipate within a very short time. A number of sensitivity tests are carried out and the
265 result suggests that the steady-state assumption is not a good assumption over the narrow

mountain ridge and valley area as shown in the Pigeon River basin. In order to compare coincident satellite rainfall retrievals and surface radar data, we will first take advantage of the comparison among the three surface radar rainfall products to get a better understanding of characteristics and weakness of Q2rad against Q2+. By assuming that the overestimation/underestimation for different rain event ensembles between Q2rad and Q2+ are similar at 5-minute and 1-h intervals, we collocated the original 5-minute Q2rad derived from radar Hybrid Scan Reflectivity (HSR) with instantaneous PR and TMI rainfall pixels to infer statistical characteristics of satellite rainfall estimation. Evaluation of PR and TMI data against Q2rad data are conducted at 5-km resolution as a function of rain intensity. The collocation is conducted by simply averaging high-resolution Q2rad data onto each sensor's footprint pixel at 5-km resolutions.

3. Comparisons of surface radar products

Figure 3 compares the distribution of annual mean rainfall from Q2rad, and Q2rad_GC, with the reference data Q2+ over the Pigeon River basin. The Q2rad product, without any gauge corrections, shows a relatively uniform rainfall field within the basin while the Q2rad_GC displays slightly larger spatial variability. The Q2+ product, on the other hand, exhibits critical variability with apparent ridge-valley gradients. In addition, the Q2+ total indicates an area of high mean precipitation extending northwest to southeast, corresponding well with major mountain ridges of the Pigeon River basin as shown in USGS SRTM elevation data. Over the Pigeon River basin and the minor ridge area on the other side of the basin, the mean precipitation amount is generally low (below 3 mmd^{-1}). The radar-only Q2rad and the gauge-corrected Q2rad_GC underestimate with respect to the Q2+ product over the major mountain ridges. This underestimation may

result from a number of factors including the limited number of gauges available for correcting the Z-R relationship over mountains, undetected low-level precipitation under the radar beam, and radar beam blocking by mountains. This underestimation is similar to that found in Tao and Barros (2013) comparing operational Q2 rainfall products with individual GSMRGN gauges over the mountains. The Q2rad_GC result does, however, do a slightly better than Q2rad over the major mountain ridges, probably due to the inclusion of a few HADS gauge records used in the bias correction process. For example, the normalized underestimation of Q2rad against Q2+ is around 20-40% along the major ridges, but the underestimation is reduced to below 20% in Q2rad_QC. Similar patterns can also be observed during both summer and winter seasons (not shown), although the wintertime precipitation amount is much smaller. On the other hand, the differences of rain amount over the Pigeon River basin and the minor mountain ridges are generally small.

Although it is difficult to quantitatively estimate errors for each individual factors contributing to the conventional radar rainfall underestimation over the mountainous areas, potential error sources related to the undetected low-level precipitation beneath the ground radar beam can be examined. For instance, the local surface radar site KMRX in Knoxville, Tennessee (as shown in Figure 1) is about 80 km away from the center of the study area. According to the National Weather Service WSR-88D radar operational procedure, a radar performs volume scans at elevation angles of 0.5º, 1.5º, 2.5º, 3.5º, 4.5º, up to 19.5º in precipitation mode. Considering that the elevation of the major mountain ridge is about 1800 m which has a radar elevation angle of 1.7º, the lowest radar beam height (above the ground) is about 0.6 km at the northwest edge and 1.5 km at the center

312 of the studied mountain ridge area after subtracting the radar elevation from the local
313 elevation and taking into account the curvature of the Earth. Therefore, many low-level
314 precipitation with echo tops below the distance-dependent radar beam elevation may not
315 be detected by the radar.

316 The frequency of rain occurrence, calculated as the ratio of the number of raining
317 samples to the total number of samples, is another way to examine the climatology of
318 rainfall characteristics. Figure 4 examines mean frequency of rain occurrence derived
319 from the three surface radar rainfall products using data from 2009 to 2011. The gauge-
320 enhanced Q2+ data show a maximum on the northwest corner and a lesser maximum in
321 the southeast corner of the domain. Both Q2rad and Q2rad_GC underestimate Q2+ over
322 most of the mountain area, with greater underestimation near the above two corners and
323 along the major mountain ridges. Q2rad_GC again performs better than Q2rad when
324 comparing against Q2+.

325 In order to further examine the contributions of rain samples within different rain
326 intensity ranges to the difference in total rain occurrence and total rain amount, the region
327 was divided into ridges and valleys according to the SRTM elevation data, and rainfall
328 event statistics evaluated as a function of rain intensity. Since the major mountain ridges
329 on the west side of the Pigeon River basin consistently showed large differences among
330 the different Q2 rainfall products and most GSMRGN gauges are located near the major
331 mountain ridges, our analysis focused on the area of major mountain ridges.

332 Figure 5 shows the frequency of rain occurrence over mountain ridges (SRTM
333 elevation >1200 m) as a function of rain intensity for the three surface radar rainfall
334 products. During the summer, the mountainous region usually features large contributions

335 from vigorous convective precipitation. Both Q2rad and Q2rad_GC appear to
336 underestimate the frequency of intermediate and heavy rain occurrence (rain intensity
337 larger than 3 mmh^{-1}), but overestimate light rain occurrence (rain intensity smaller than 3
338 mmh^{-1}). This phenomenon may be associated with the underestimation of rain intensity in
339 Q2rad and Q2rad_GC over mountain ridges: Some of the intermediate and heavy rain
340 events shown in Q2+ may be classified in Q2rad and Q2rad_GC as rain events with
341 lighter rain intensities. Another possible explanation for the overestimation of light rain
342 events is that radar rain retrieval algorithm used during summertime is not able to handle
343 convection over mountain ridges. The limited conventional rain gauge data utilized in
344 Q2rad_GC are mainly located in low-elevation areas where annual rain accumulation is
345 small. The distinctly different precipitation characteristics between ridges and valleys
346 during the summer may not help to correct bias near mountain ridges. For very heavy rain
347 events, the three rainfall products tend to agree well in terms of frequency of rain
348 occurrence.

349 During the winter, persistent, light stratiform precipitation provides large
350 contributions to the total precipitation (Wilson and Barros 2014). The frequency of heavy
351 rain events is significantly reduced in all three radar rainfall products. Both Q2rad and
352 Q2rad_GC significantly underestimate the incidence of light rain events and moderately
353 underestimate incidence of intermediate rain events. This suggests a problem in the
354 detection of wintertime precipitation resulting from the radar retrieval algorithm. It is
355 interesting to notice that Q2rad_GC appears to agree slightly better with Q2+ than Q2rad
356 for rain events with intensities above 3 mmh^{-1}, possibly due to some bias correction

357 effects from rain gauges located in low-elevation areas (i.e. HADS) which may have
358 similar rain characteristics to those over ridges.

359 Figure 6 compares fraction of rain amount as a function of rain intensity over
360 mountain ridges from the three radar rainfall products. During the summer, some
361 intermediate and heavy rain samples are identified as lighter rain samples in the Q2rad
362 and Q2rad_GC. The Q2rad and Q2rad_GC therefore slightly overestimate the total of
363 light rainfall but greatly underestimate the total at intermediate and heavy rain intensities.
364 The largest rain amount underestimation occurs with rain rates between 5 and 20 mmh^{-1},
365 with about 30% underestimation. During the winter, Q2rad underestimates Q2+ rainfall
366 total throughout all the rain intensity ranges. Q2rad_GC also underestimates Q2+ rainfall
367 total for light rain events and some intermediate rain intensities (rain rates less than 6
368 mmh^{-1}). For rain intensities greater than 6 mmh^{-1}, the Q2rad_GC appears to agree better
369 with Q2+ than Q2rad, indicating some influence of bias-correction from a limited number
370 of conventional gauges at low-elevations.

371 The above comparisons of the rain occurrence and fraction contribution to the rain
372 amount illustrate the collective impact of factors such as the limited number of gauges
373 available for correcting the Z-R relationship over the mountains, undetected low-level
374 precipitation under radar beam elevation, and radar beam blocking by the terrain. Figure
375 7 shows the joint distribution of coincident rain occurrence between the Q2+ and the
376 other two radar rainfall products during summer and winter over mountain ridges. This
377 kind of plot is similar to scatter plots but instead of showing the collocated raining
378 samples, it displays the accumulated distribution of coincident sample numbers. Both the
379 Q2rad and Q2rad_GC data generally agree with the Q2+ during both summer and winter.

However, careful examination indicates that the collocated Q2rad data appear to slightly overestimate rain intensity for very light rain events and underestimate rain intensity for intermediate and heavy rain events. Small improvements can be noticed in the Q2rad_GC data especially for heavy rain events and very light rain events. The bias correction, although coming from gauges some distance away from mountain ridges, does help to obtain better rainfall estimates over the data-sparse ridge area if the two areas feature similar rain characteristics.

Large mountain ridges and valleys usually have distinctly different diurnal variations of precipitation (e.g., Astling 1984; Riley et al. 1986). During the warm season, mountain ridges warm up quickly during the day due to the dominant daytime boundary layer heating, and strong convection usually occurs in the afternoon. On the other hand, mountain valleys cool much more slowly than ridges during the night, and the local ridge-valley circulation usually leads to late night precipitation in valleys. Figure 8 compares diurnal variation of precipitation features over mountain ridges during the summer from the three radar rainfall products. Consistent with earlier studies, the occurrence of and contribution to the total rainfall all indicate a single peak in the afternoon between 13 and 15 LST over mountain ridges. The Q2rad_GC appears to have very similar diurnal signals as the Q2+ in terms of frequency of rain occurrence while Q2rad overestimates rain occurrence from early afternoon to late evening. This overestimation in the Q2rad may be associated with light rain detection from the unadjusted radar retrieval scheme. On the other hand, the Q2rad and Q2rad_GC agree very well in terms of diurnal variation of rain amount and both of them underestimate the Q2+ from morning to afternoon. This underestimation, as discussed earlier, may come

403 from underestimated rain intensity from intermediate and heavy rain events. The narrow
404 valley area in the Pigeon River basin is strongly modulated by convection on the
405 mountain ridge. All three radar rainfall products exhibit a similar diurnal precipitation
406 pattern as the ridge with a single rainfall peak in the afternoon (not shown). However, for
407 extensive valley areas which may show a distinctly different diurnal rain features, using
408 gauge data in valley areas to perform bias corrections over the data-scarce ridge areas
409 could lead to even larger uncertainties, especially for transient small- and mesoscale
410 precipitating systems.

411 In summary, the statistical evaluations of two experimental surface radar rainfall
412 products against a gauge-enhanced radar rainfall product over mountain regions show a
413 reasonably good agreement among these surface radar rainfall data in terms of rain
414 occurrence and rain amount. The diurnal signals of precipitation over mountain ridges
415 are well captured and joint distributions of coincident raining samples agree well. The
416 rain intensity bias and light rain detection associated with the radar retrieval schemes and
417 the impact of the mountains are clearly noticed. Comparing with the reference Q2+ which
418 merges both enhanced gauge data in high-elevations areas and conventional gauge data in
419 mid- to low-elevation areas, the Q2rad tends to underestimate rain occurrence and rain
420 amount at intermediate and heavy rain intensities, and during summer it also
421 overestimates rain occurrence and rain amount for light rain intensities. The Q2rad_GC,
422 which merges limited conventional gauge data located in mid- to low elevation areas, to
423 some extent may help to improve rainfall estimations over data-sparse areas but the result
424 is highly dependent on the similarity of precipitation characteristics between gauge
425 locations and the remote mountain areas.

426

427 # 4. Comparisons with satellite rain retrievals

428 Analyses in Section 3 provide many statistical characteristics for hourly
429 surface radar rainfall products over mountainous regions, particularly the difference
430 between the Q2rad and the Q2+ products. Although surface radar-gauge merged rainfall
431 products currently do not have temporal resolutions less than 1 hour, we can coincidently
432 compare the original Q2rad at 5-minute intervals with instantaneous satellite rainfall
433 retrievals to meet the requirement of collocation at the satellite rainfall product
434 resolution.

435 Figure 9 examines the distribution of summertime mean satellite rainfall
436 retrievals vs. the sensor swath-sampled Q2rad on a 0.1°x0.1° grid. Although the data are
437 accumulated for three summers, the satellite revisit numbers are still not sufficient to
438 compare with fully-sampled rainfall distributions similar to that shown in Figure 3. Since
439 the PR and TMI have different swaths, their sample sizes are different, consequently we
440 can only compare retrievals from each sensor with the sensor-sampled Q2rad product.
441 The spatial distributions of PR and PR-sampled Q2rad rainfall show similar patterns with
442 a maximum near the southeast corner of the domain and a minimum on the northwest
443 side. Except for a small area near the right hand side of the domain showing some
444 overestimation, the Q2rad in general underestimates compared to the PR over most of the
445 mountain areas, with the largest underestimation located near the main mountain ridge.
446 The TMI and TMI-sampled Q2rad products indicate similar spatial rainfall distributions
447 with a maximum on the northwest part of the domain but also with a few discrepancies.
448 As discussed in many earlier studies (e.g., Wilheit 1986; Kummerow et al. 2001; Ferraro

449 et al. 2005), passive microwave rain estimates over land are still largely empirically
450 retrieved from scattering-based algorithms and have significant uncertainties. Not only is
451 the scattering of microwave radiation highly dependent on the poorly known details of
452 the ice-size distribution, but also the precipitation estimate is primarily related to frozen
453 hydrometeor aloft which has a less direct relationship with surface rain rates. Highly
454 variable land surface such as mountain ridges and valleys further make it difficult to
455 distinguish rainfall pixels over complicated and varied surface backgrounds.

456 During the wintertime (Figure 10), except near the southwest corner where the PR
457 clearly overestimates, the PR and PR-sampled Q2rad indicate a similar distribution with
458 maxima in northwest and southeast corners. Over other parts of the domain, the Q2rad
459 tends to overestimate compared to the PR. The TMI-sampled Q2rad also shows a rain
460 distribution similar to the PR-sampled Q2rad. However, the TMI has significant
461 problems in retrieving wintertime precipitation over mountainous regions with very small
462 rain amounts across the whole domain. It is likely the current empirical retrieval
463 algorithm has difficulties retrieving precipitation over snow-covered regions and solid or
464 mixed precipitation.

465 Figure 11 shows the frequency of rain occurrence as a function of rain intensity
466 over mountain ridge. During the summer, the PR significantly underestimates the
467 occurrence of light rainfall compared to the PR-sampled Q2rad, mainly due to PR's
468 detection capability (PR's minimum detectable rain rate is 0.5-0.7 mmh^{-1}). For
469 intermediate and heavy rain intensities, PR generally overestimates the rainfall
470 occurrence compared to the Q2rad product. Considering Figure 5 which shows the Q2rad
471 suffers less rain occurrence over mountain ridges, the PR data may be closer to the

472 reference in observing intermediate and heavy rain intensities. The TMI also has large
473 underestimates for light rain intensities since the minimum detectable rain rate for the
474 TMI GPROF algorithm over land is about 1 mmh^{-1}. For intermediate and heavy rain
475 events, the TMI detects more rain occurrences than the Q2rad, which is consistent with
476 the PR data. During the winter, the PR cannot detect most light rain intensities below 1
477 mmh^{-1}, but can still detect more rain occurrence than the Q2rad for rain events with rain
478 intensities above 4 mmh^{-1}. The TMI however, shows a distinctly different pattern in the
479 occurrence of rainfall since it cannot detect any rain intensities below 1.0 mmh^{-1}, and
480 above 6 mmh^{-1}. This issue reflects the fact that the current GPROF algorithm over land
481 has significantly large space for improvement to retrieve wintertime precipitation over
482 mountain areas.

483 The contribution of rain intensities to the total rainfall amount is shown in Figure
484 12. This indicates that during the summer both PR and TMI tend to overestimate with
485 respect to the corresponding Q2rad at intermediate and heavy rain intensities and
486 underestimate Q2rad at light rain intensities. These are similar to the statistical features
487 shown in Figure 6 which compared Q2+ to Q2rad. During the winter, the PR also
488 indicates similar features as in the summer but the TMI has retrieval problems and can
489 only provide rain estimates within a very narrow range of rain intensities. Joint
490 distributions of coincident raining sample numbers (Figure 13) also suggest that the PR
491 agrees well with the Q2rad during both summer and winter, and the PR generally
492 overestimates compared to the Q2rad at intermediate and heavy rain intensities at the 5
493 km footprint scale. The TMI product is similar to that of the Q2rad during the summer

494 with small overestimates but can only retrieve rain estimates between 1 and 4 mmh^{-1}
495 during winter.
496

497 # 5. Summary

498 Due to the highly variable precipitation features associated with topography
499 and the limitation of sensors in their coverage and measuring capabilities, accurate
500 estimations of precipitation over mountain areas at fine temporal and spatial resolutions
501 has been a challenging task. Although the commonly-used surface rain reference data
502 from conventional gauge and ground radar network have provided many insights in
503 weather analysis and forecast, they have large biases over mountainous regions and
504 therefore cannot be used as a perfect reference. Satellite rainfall retrievals also have
505 significant uncertainties over land, particularly over complicated mountainous regions
506 such as the Appalachians (Prat and Barros 2010; Duan et al. 2015). Following Tao and
507 Barros (2013) a new hourly surface radar rainfall product merging a conventional gauge-
508 adjusted radar rainfall product (Zhang et al. 2011) with the very dense rain gauge
509 observations has been developed over the Pigeon River basin in the Southern
510 Appalachian Mountains.

511 In this study, the gauge-enhanced rainfall product is used to evaluate the
512 performance of two operational surface radar rainfall products (radar-only Q2rad and
513 conventional gauge-adjusted Q2rad_GC). Relative to the 5 conventional gauges which
514 are located in the low-elevation river basin area, the enhanced gauge stations are mainly
515 installed in high-elevation regions, and provide a good opportunity to evaluate rainfall
516 estimates over mountain ridges. Rain detection and statistical differences of these three

surface radar rainfall products are examined as a function of rain intensity in different seasons. By defining each data at 0.01^{o}x0.01^{o} horizontal resolutions and 1-h temporal resolutions as an individual precipitating/non-precipitating sample, statistics of rain occurrence and rain amount including their geographical and seasonal variations is documented over a 3-year period between 2009 and 2011.

The results show that there is a reasonably good statistical agreement among these surface radar rainfall data over mountainous regions in terms of horizontal mean distributions of rain occurrence and amount. The fraction of rain occurrence and fraction of rain amount also indicate similar distribution patterns as a function of rain intensity. The diurnal signals of precipitation over mountain ridges are well captured and joint distributions of coincident raining samples indicate similarities during both summer and winter.

However, biases in rain intensity, frequency of occurrence, and rain detection are also clearly noticed. The rain uncertainties are the collective result from a number of factors including the limited number of gauges available for correcting the Z-R relationship over mountains, undetected low-level precipitation under radar beam elevation, and radar beam blocking by mountains. Comparing with the reference Q2+ (which has enhanced gauge observations in high-elevation areas), both the Q2rad and the Q2rad_GC tend to underestimate rain occurrence and rain amount at intermediate and heavy rain intensities and overestimate rain occurrence and rain amount at light rain intensities during the summer. Some of the intermediate and heavy rain intensities shown in Q2+ may be classified in the Q2rad and Q2rad_GC as rain events with lighter rain intensities. The Q2rad_GC product may help to improve rainfall estimates over data-

sparse mountainous areas but the result is highly dependent on the similarity of precipitation characteristics at the gauges and the rainfall regimes in remote mountainous areas. Over the Pigeon River basin, for example, a limited number of conventional gauge stations are installed in low-elevation areas for hydrologic purposes. However, even as this number is small, because the valleys occupy a relative small fraction of the inner mountain region, and despite significant differences between rainfall on adjacent ridges and valleys on an event basins (e.g. Wilson and Barros, 2014; Duan et al. 2015), the use of low elevation gauges to correct radar rainfall estimates proves to be useful from the point of view of the bulk statistics examined here. Over large mountain areas where there are distinctly different diurnal precipitation features over ridges and valleys, using conventional gauge data observed near the valley to correct radar rainfall bias on the ridge could incorporate more uncertainties in rainfall estimates than the original radar-only product, and the diurnal rainfall signals could even be erroneously modified. Great care should be taken with the representativeness error when using the conventional gauge-adjusted radar rainfall product over mountain areas.

With a better understanding of surface radar hourly rainfall products over mountain areas, we coincidently compared the original Q2rad at 5-minute intervals with instantaneous satellite rainfall retrievals from TRMM PR and TMI at their rain footprint resolutions. By assuming that the 5-minute and 1-hour Q2rad data suffer similar topographical impacts over mountain areas, we can indirectly infer some statistical features of satellite rainfall retrievals, especially the one derived from the PR data.

It is found that the horizontal mean rainfall distributions of the PR and PR-sampled Q2rad have similar patterns during both summer and winter. The PR

563 overestimates rainfall compared to the Q2rad rainfall near mountain ridges in a similar
564 way to the Q2+, especially during the summer. The TMI and TMI-sampled Q2rad show
565 similar horizontal rainfall distributions during the summer but with large differences.
566 During the winter, the GPROF7 PMW rain algorithm has problems in retrieving
567 precipitation over mountainous regions, resulting in very low rain amounts across the
568 whole domain. This reflects a fact that the current empirical retrieval algorithm is not
569 able to handle light rainfall which is dominant in the Appalachians in the cold season, as
570 well snow-covered mountainous regions and solid precipitation.

571 Comparisons of PR and Q2rad indicate that the PR and PR-sampled Q2rad are
572 in reasonably good agreement in terms of the frequency of rain occurrence and fraction of
573 rain amount. The PR significantly underestimates incidence of light rain intensities
574 compared to the PR-sampled Q2rad, mainly due to PR's detection capability (PR's
575 minimum detectable rain rate is 0.5-0.7 mmh^{-1}; see Duan et al. (2015) for a detailed study
576 of PR error characteristics in the Southern Appalachians). The recently-launched DPR on
577 board the GPM core satellite has a minimum detectable rain rate around 0.3 mmh^{-1}, it is
578 therefore expected that light rain intensities can be better retrieved in DPR. For
579 intermediate and heavy rain events, the PR in general overestimates rain occurrence and
580 rain amount compared to that of the Q2rad product. Considering that the Q2+ also
581 overestimates compared to that of the Q2rad product in rain occurrence and rain amount,
582 the PR data appears to be statistically more close to the reference in detecting and
583 estimating intermediate and heavy rain intensities.

584 Satellite microwave rainfall retrievals have been widely used to provide rainfall
585 estimates on the global scale. Among these microwave instruments, space-borne

586 precipitation radars have long been expected to serve as space-borne rain references for
587 assessing other satellite rainfall retrievals and even some surface measurements. In this
588 study, we have showed the potential that PR may perform equally well and sometimes
589 better than the high-resolution radar-only rainfall product over complicated terrain for
590 intermediate and heavy rain intensities. After careful calibration and with good reference
591 data, space-borne precipitation radars will indeed be able to serve as a "flying rain gauge"
592 to assess not only other satellite rainfall retrievals, but also surface measurements over
593 data-sparse regions (Hou et al. 2014).
594

Acknowledgements.

The surface radar rainfall products are obtained from NOAA NSSL and University of Oklahoma. This research is supported by the GPM Project at the NASA Goddard Space Flight Center in Greenbelt, MD and a NASA funding NNX13AG50G.

References

Astling, E. G., 1984: On the relationship between diurnal mesoscale circulations and precipitation in a mountain valley. *Journal of Climate and Applied Meteorology*, 23, 1635-1644.

Barros, A. P., Joshi, M., Putkonen, J., and Burbank, D. W., 2000: A study of the 1999 monsoon rainfall in a mountainous region in central Nepal using TRMM products and rain gauge observations. Geophys. Res. Lett, 27, 3683-3686.

Chen, S., and Coautors, 2015: Inter-comparison of Precipitation Estimates from WSR-88D Radar and TRMM Measurement over Continental United States. IEEE Transactions on Geoscience and Remote Sensing, DOI: 10.1109/TGRS.2015.2399307.

Duan, Y., A. M. Wilson, A.M., and A. P. Barros, 2015: Scoping a Field Experiment: Error Diagnostics of TRMM Precipitation Radar Estimates in Complex Terrain as a basis for IPHEx2014. *Hydrol. Earth Sys. Sci.*, in press.

Ferraro, R. R., E. A. Smith, W. Berg, and G. J. Huffman, 1998: A screening methodology for passive microwave precipitation retrieval algorithms. J. Atmos. Sci., 55, 1583-1600.

626 Ferraro, R. R., F. Weng, N. C. Grody, L. Zhao, 2000: Precipitation characteristics over
627 land from the NOAA-15 AMSU sensor. Geophysical Research Letters, 27, 2669-
628 2672.
629
630 Ferraro, R. R., F. Weng, N. C. Grody, L. Zhao, H. Meng, C. Kongoli, P Pellegrino, S.
631 Qiu, and C. Dean, 2005: NOAA operational hydrological products derived from the
632 advanced microwave sounding unit. IEEE Transactions on Geoscience and Remote
633 Sensing, 43, 1036-1049.
634
635 Hou, A. Y., and Coauthors, 2014: The Global Precipitation Measurement Mission.
636 *Bulletin of the American Meteorological Society*, 95, 701-722.
637
638 Iguchi, T., T. Kozu, R. Meneghini, J. Awaka, K. Okamoto, 2000: Rain-profiling
639 algorithm for the TRMM precipitation radar. Journal of Applied Meteorology, 39,
640 2038-2052.
641
642 Kim, D., B. Nelson, D.-J. Seo, 2009: Characteristics of Reprocessed
643 Hydrometeorological Automated Data System (HADS) Hourly Precipitation Data.
644 *Weather and Forecasting*, 24, 1287-1296.
645
646 Krakauer, N. Y., S. M. Pradhanang, T. Lakhankar, and A. K. Jha, 2013: Evaluating
647 satellite products for precipitation estimation in mountain regions: A case study for
648 Nepal. Remote Sensing, 5, 4107-4123.

649

650 Kummerow, C., W. S. Olson, and L. Giglio, 1996: A simplified scheme for obtaining
651 precipitation and vertical hydrometeor profiles from passive microwave sensors.
652 IEEE Trans. Geosci. Remote Sens., 34, 1213-1232.

653

654 Kummerow, C., W. Barnes, T. Kozu, J. Shiue, and J. Simpson, 1998: he Tropical
655 Rainfall Measuring Mission (TRMM) sensor package. J. Atmos. Oceanic Technol.,
656 15, 809-817.

657

658 Kummerow, C., and Coauthors, 2000: The status of the Tropical Rainfall Measuring
659 Mission (TRMM) after two years in orbit. Journal of Applied Meteorology, 39, 1965-
660 1982.

661

662 Kummerow, C., Y. Hong, W. S. Olson, S. Yang, R. F. Adler, J. McCollum, R. Ferraro,
663 G. Petty, D.-B. Shin, and T. T. Wilheit, 2001: The evolution of the Goddard profiling
664 algorithm (GPROF) for rainfall estimation from passive microwave sensors. J. Appl.
665 Meteor., 40, 1801-1820.

666

667 Kummerow, C., S. Ringerud, J. Crook, D. Randel, W. Berg, 2011: An Observationally
668 Generated A Priori Database for Microwave Rainfall Retrievals. *Journal of*
669 *Atmospheric and Oceanic Technology*. 28, 113-130.

670

671 Masunaga, H., T. Iguchi, R. Oki, and M. Kachi. 2002: Comparison of Rainfall Products
672 Derived from TRMM Microwave Imager and Precipitation Radar**.** *Journal of Applied*
673 *Meteorology*: 41, 849–862.
674
675 Masunaga, H. and C. D. Kummerow, 2005: Combined radar and radiometer analysis of
676 precipitation profiles for a parametric retrieval algorithm, *J. Atmos. Oceanic*
677 *Technol.*, **22**, 909-929.
678
679 Meneghini, R., and T. Kozu, 1990: Spaceborne Weather Radar. Artech House, Boston,
680 197 pages.
681
682 Nelson, B. R., D.-J. Seo, D. Kim, 2010: Multisensor Precipitation Reanalysis. *Journal of*
683 *Hydrometeorology*, 11, 666-682.
684
685 Olson, W. S., C. Kummerow, Y. Hong, and W.-K. Tao, 1999: Atmospheric latent heating
686 distributions in the Tropics derived from satellite microwave radiometer
687 measurements. J. Appl. Meteor., 38, 633-664.
688
689 Olson, W. S. C. D. Kummerow, S. Yang, G. W. Petty, W.-K. Tao, T. L. Bell, S. A.
690 Braun, Y. Wang, S. E. Lang, D. E. Johnson, and C. Chiu, 2006: Precipitation and
691 latent heating distributions from satellite passive microwave radiometry. Part I:
692 Improved method and uncertainties. Journal of Applied Meteorology and
693 Climatology, 45, 702-720.

694

695 Prat, O. P., and A. P., Barros, 2010: Assessing satellite-based precipitation estimates in
696 the Southern Appalachian Mountains using rain gauges and TRMM PR, Advances in
697 Geosciences, 25, 143-18 153, 10.5194/adgeo-25-143-2010.

698

699 Riley, G. T., M. G. Landin, and L. F. Bosart, 1987: The diurnal variability of
700 precipitation across the Central Rockies and adjacent Great Plains. Mon. Wea. Rev.,
701 115, 1161-1172.

702

703 Seo, D.-J., 1998: Real-time estimation of rainfall fields using rain gauge data under
704 fractional coverage conditions. J. Hydrol., 208, 25-36.

705

706 Seo, D.-J., J. Breidenbach, R. Fulton, D. Miller, and T. O'Bannon, 2000: Real-time
707 adjustment of range-dependent biases in WSR-88D rainfall estimates due to
708 nonuniform vertical profile of reflectivity. J. Hydrometeor., 1, 222–240.

709

710 Simpson, J., R. F. Adler, and G. R. North, 1988: A proposed Tropical Rainfall Measuring
711 Mission (TRMM) satellite. *Bull. Amer. Meteor. Soc*., 69, 278-295.

712

713 Simpson, J., C. Kummerow, W.-K. Tao, and R. F. Adler, 1996: On the tropical Rainfall
714 Measuring Mission (TRMM). *Meteor. Atmos. Phys*., 60, 19-36.

715

716 Tao, J., and A. P. Barros, 2013: Prospects for flash flood forecasting in mountainous
717 regions – An investigation of Tropical Storm Fay in the Southern Appalachians. J.
718 Hydrol., 506, 69-89.
719
720 Vasiloff, S. V., and Coauthors, 2007: Improving QPE and very short term QPF: An
721 initiative for a community-wide integrated approach. Bull. Amer. Meteor. Soc., 86,
722 1899-1911.
723
724 Wallace, J. M., 1975: Diurnal variations in precipitation and thunderstorm frequency over
725 the conterminous United States. Mon. Wea. Rev., 103, 406-419.
726
727 Ware, E. C., 2005: Corrections to radar-estimated precipitation using observed rain gauge
728 data. M.S. thesis, Cornell University, 87 pp. [Available from Cornell University
729 Library, 201 Olin Library, Cornell University, Ithaca, NY 14853-5301.].
730
731 Weng, F., L. Zhao, R. Ferraro, G. Poe, X. Li, and N. Grody, 2003: Advanced Microwave
732 Sounding Unit cloud and precipitation algorithms. *Radio Sci*., 38, 8068-8079.
733
734 Wilheit, T. T., 1986: Some comments on passive microwave measurement of rain. *Bull.*
735 *Amer. Meteor. Soc*., 67, 1226-1232.
736

737 Wilson, A.M., and A. P. Barros, 2014: An investigation of warm rainfall microphysics in
738 the Southern Appalachians: Orographic enhancement via low-level seeder-feeder
739 interactions. Journal of the Atmospheric Sciences, 71, 1783-1805.
740
741 Yamamoto, M. K., K. Ueno, and K. Nakamura, 2011: Comparison of satellite
742 precipitation products with rain gauge data from the Khumb region, Nepal
743 Himalayas. J. Meteorol. Soc. Japan, 89, 597-610.
744
745 Zhang, J. and Coauthors, 2011: National mosaic and multi-sensor QPE (NMQ) system.
746 BAMS, 92, 1321-1338.
747
748 Zhao, L., and F. Weng, 2002: Retrieval of ice cloud parameters using the Advanced
749 Microwave Sounding Unit. *J. Appl. Meteor*., 41, 384-395.

List of Tables

757

758

759 Table 1: Summary of the RMSE computed from observed rainfall rate (mmh^{-1}) and Q2
760 products before and after adjustment.

QPE	**RMSE(mmh^{-1})**			
	GSMRGN	**ECONET**	**HADS**	**All**
Q2 (Q2rad_GC)	0.64	0.59	0.54	0.63
Q2+_All*	0.44	0.39	0.40	0.43
Q2+_H/L*	0.60	0.26	0.44	0.56
Q2+_cdfThr	0.30	0.28	0.27	0.29

761
762 * Q2+_All and the Q2+_H/L are generated using the methods developed in the study of Tao and Barros
763 (2013)
764

765

766

List of Figures

790 Figure 5: Frequency of rain occurrence as a function of rain intensity during summer
791 (upper panel) and winter (lower panel) for rain events between 2009 and 2011 over
792 mountain ridges.
793
794 Figure 6: Fraction of rain amount as a function of rain intensity during summer (upper
795 panel) and winter (lower panel) for rain events between 2009 and 2011 over mountain
796 ridges.
797
798 Figure 7: Joint distributions of coincident rain sample numbers during summer and winter
799 over mountain ridges: between Q2+ and Q2rad (upper panels) and between Q2+ and
800 Q2rad_GC (lower panels).
801
802 Figure 8: Diurnal variation of rain characteristics over mountain ridges during the
803 summer. Upper panel: frequency of rain occurrence (%), lower panel: fraction of rain
804 amount (%).
805
806 Figure 9: Mean rain amount from Q2rad, PR and TMI during the summer and the
807 difference between surface radar rainfall and satellite rain retrievals.
808
809 Figure 10: Mean rain amount from Q2rad, PR and TMI during the winter and the
810 difference between surface radar rainfall and satellite rain retrievals.

Figure 11: Frequency of rain occurrence (%) as a function of rain rate over mountain ridges during summer and winter for coincident rain samples of PR and PR-sampled Q2rad, and of TMI and TMI-sampled Q2rad.

Figure 12: Same as Figure 11 but for fraction of rain amount over mountain ridges.

Figure 13: Joint distributions of coincident rain sample numbers during summer and winter over mountain ridges: between PR and Q2rad (upper panels) and between TMI and Q2rad (lower panels).

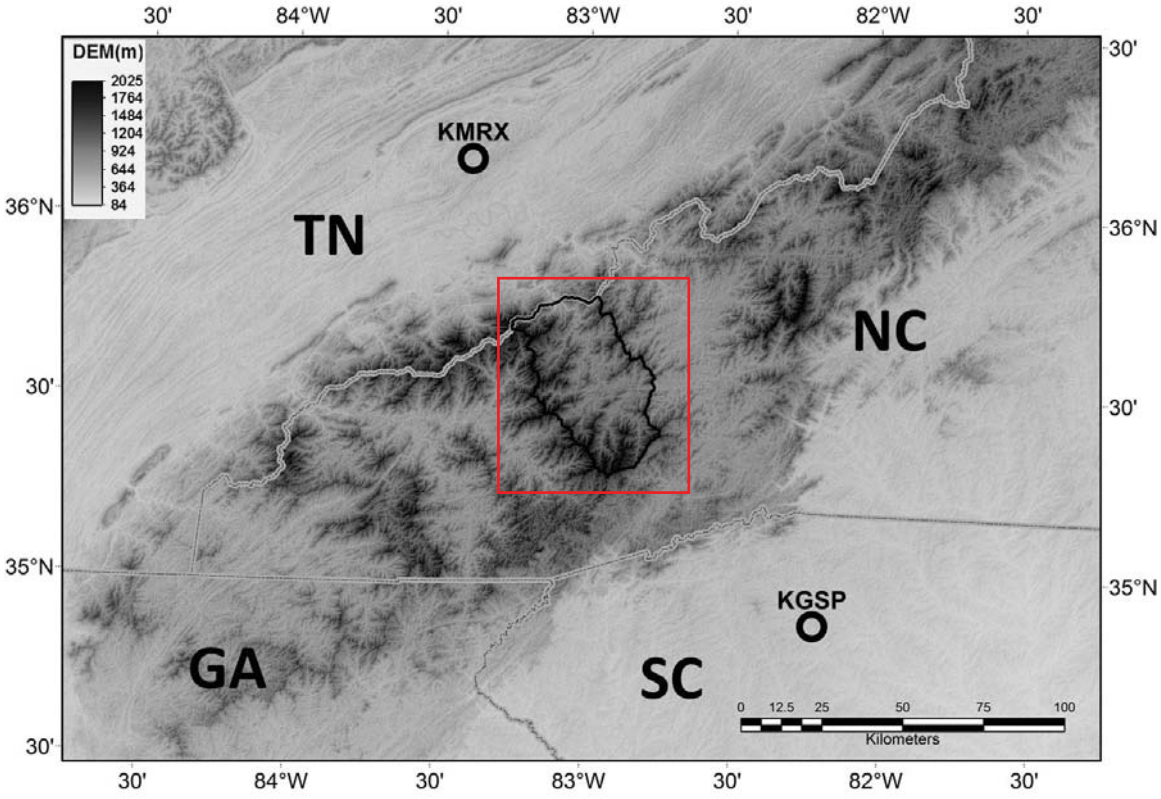

Figure 1: Locations of two conventional WSR-88D radar sites (KMRX in Knoxville/Tennessee and KGSP in Greer/South Carolina) near the Pigeon River basin (marked by heavy slid curve) in the Southern Appalachian Mountains. The rectangle in red color corresponds to the study area shown in Figure 2. TN: Tennessee; NC: North Carolina; GA: Georgia; SC: South Carolina.

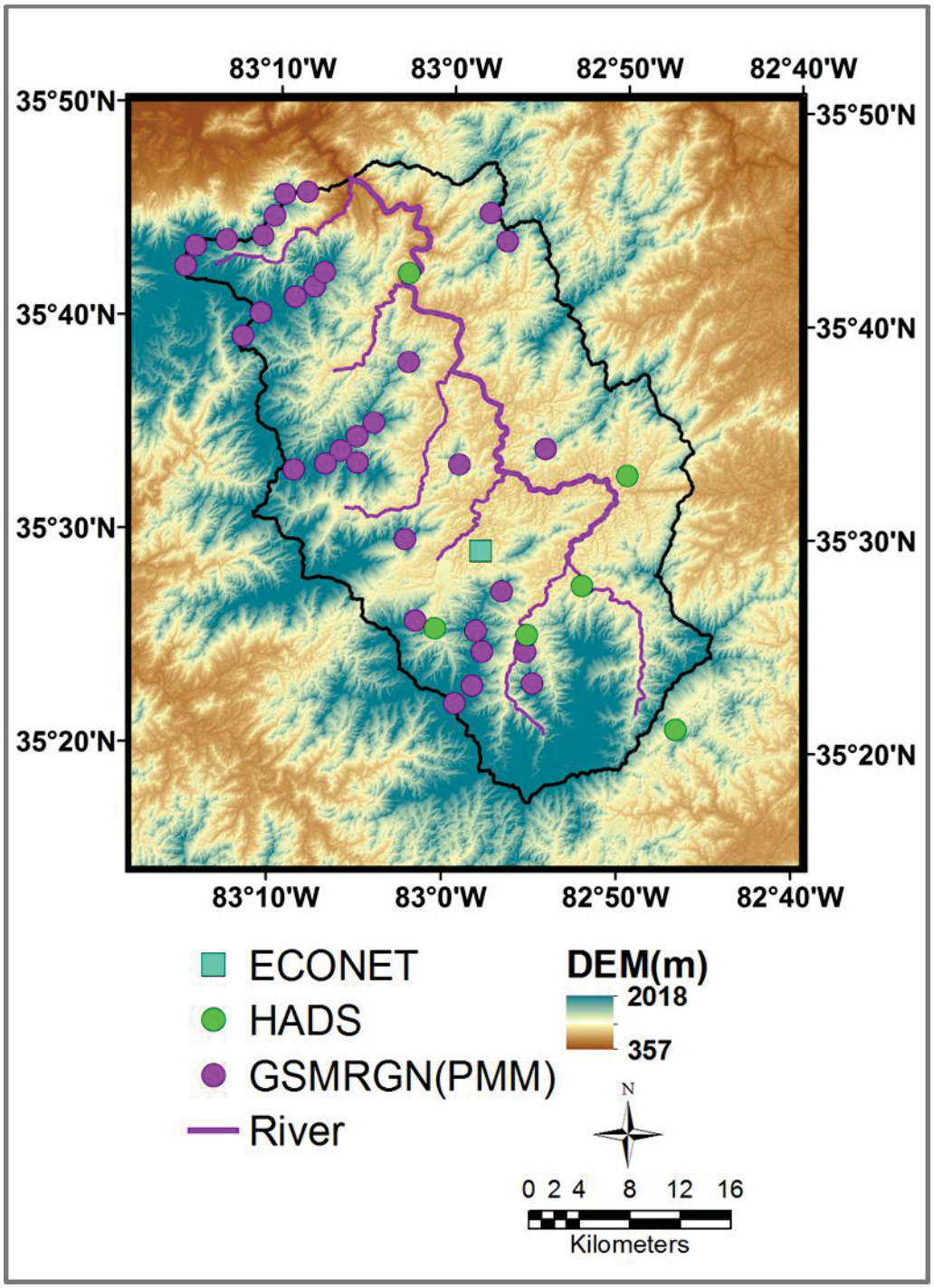

Figure 2: A topography map in the Pigeon River basin over the Southern Appalachian Mountains with blue shading indicating higher-elevation areas and yellow shading indicating lower-elevation areas. The purple curve is the Pigeon River. The green dots indicate locations of conventional Hydrometeorology Automated Data System (HADS) rain gauge stations. The purple dots are locations of Great Smoky Mountain Rain Gauge Network (GSMRGN)/Precipitation Measurement Mission (PMM) rain gauges.

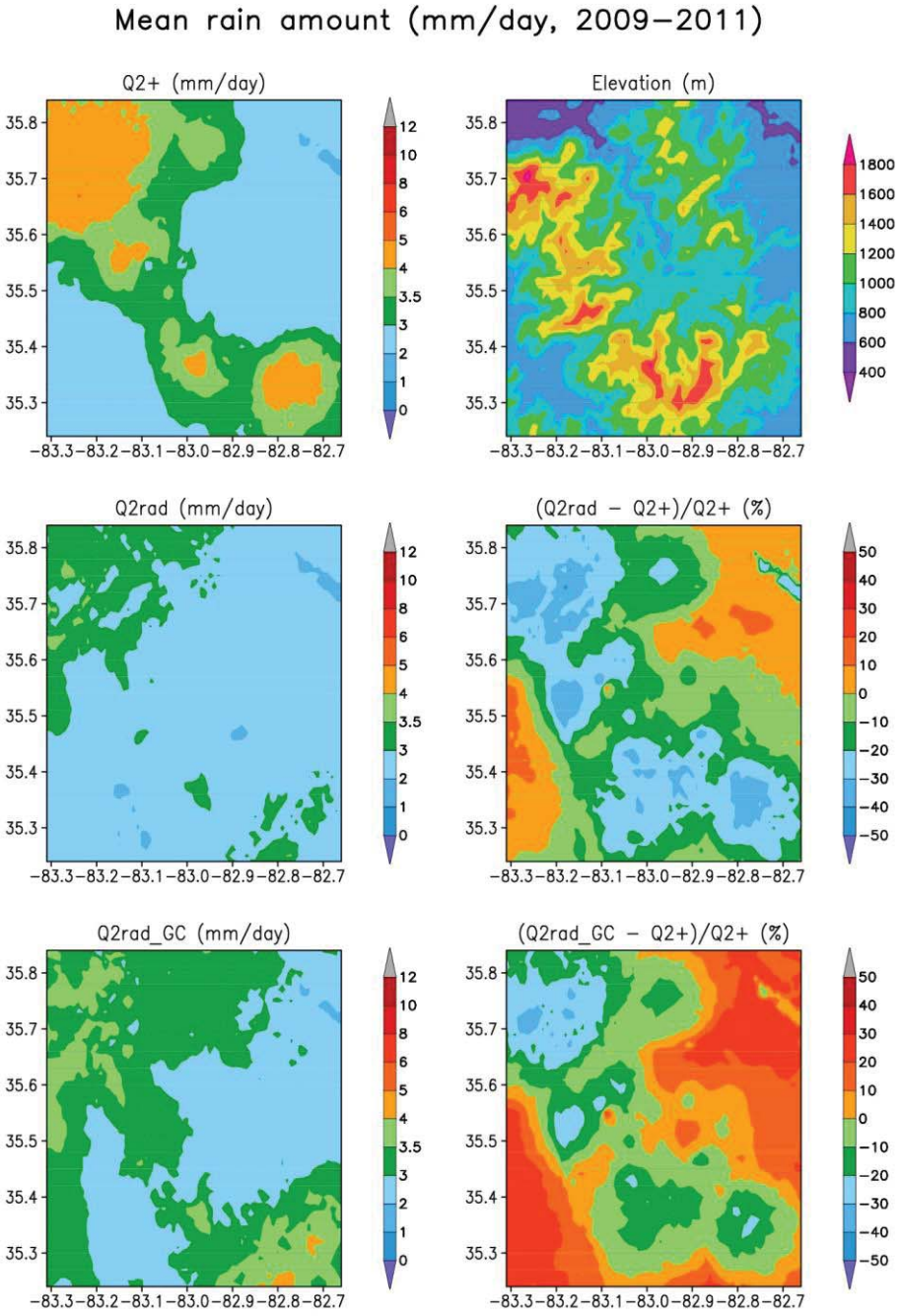

Figure 3: Annual mean rain amount from surface radar rainfall products and their normalized differences in the Pigeon River basin over the Southern Appalachian Mountains. Q2rad is the original radar-only rainfall product. Q2rad_GC is a conventional gauge-adjusted radar rainfall product. Q2+, the reference, is a special gauge-enhanced radar rainfall product. SRTM 0.01º x 0.01º elevation data derived from US Geography Survey's SRTM30 are also included to indicate mountain ridges and valleys.

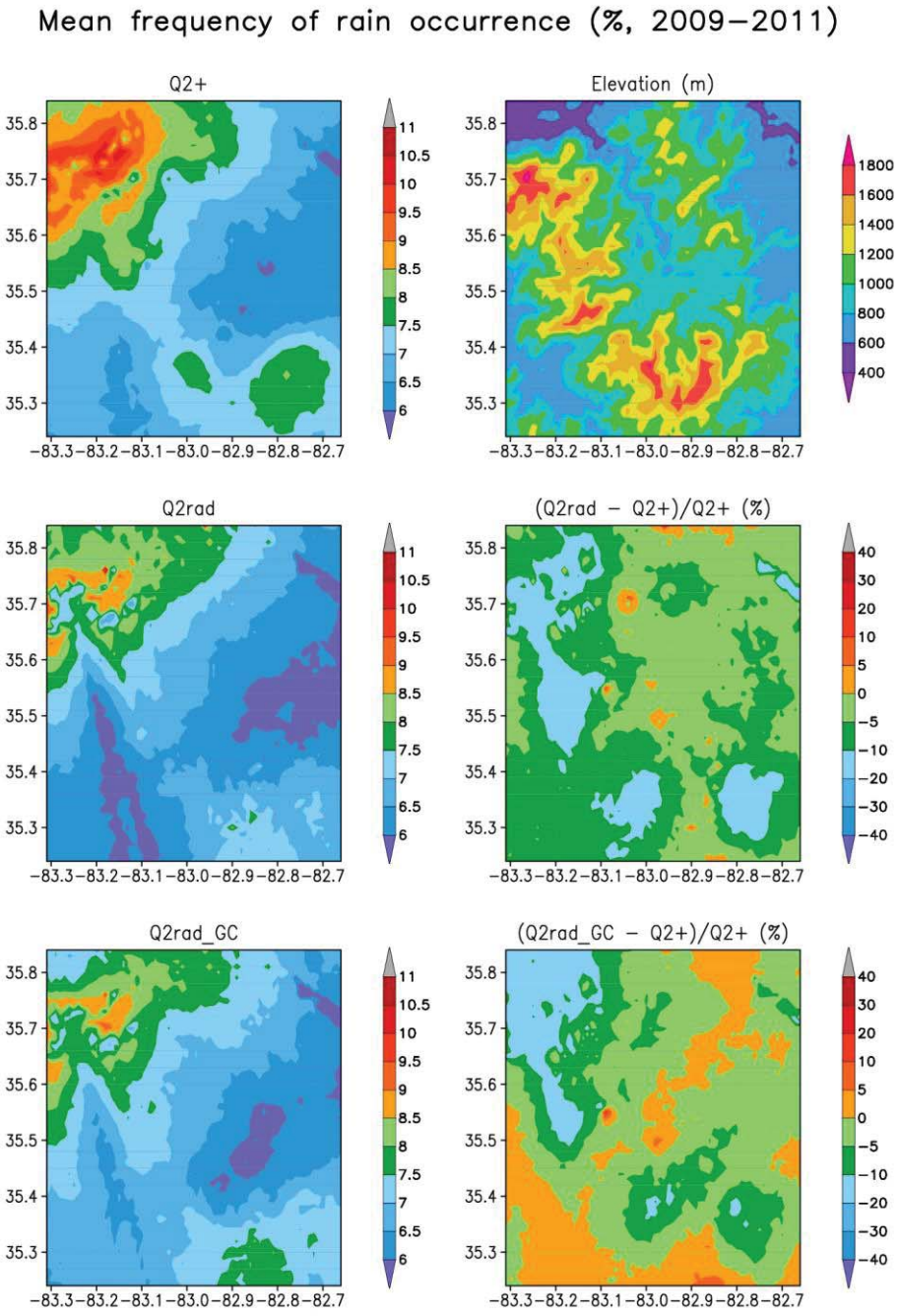

Figure 4: Same as in Figure 2 but for fraction of rain occurrence (%) and their normalized differences.

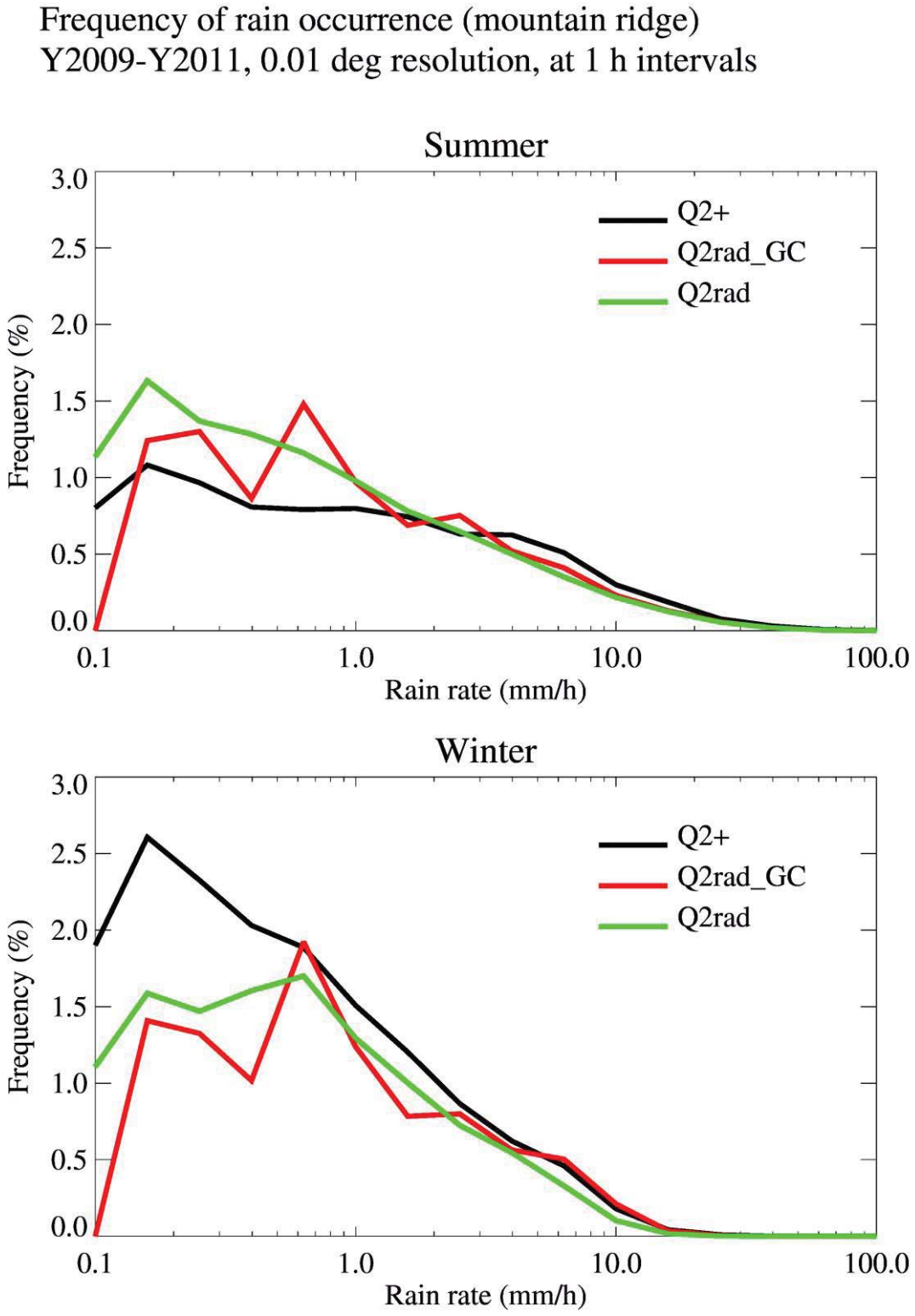

867
868 Figure 5: Frequency of rain occurrence as a function of rain intensity during summer
869 (upper panel) and winter (lower panel) for rain events between 2009 and 2011 over
870 mountain ridges.

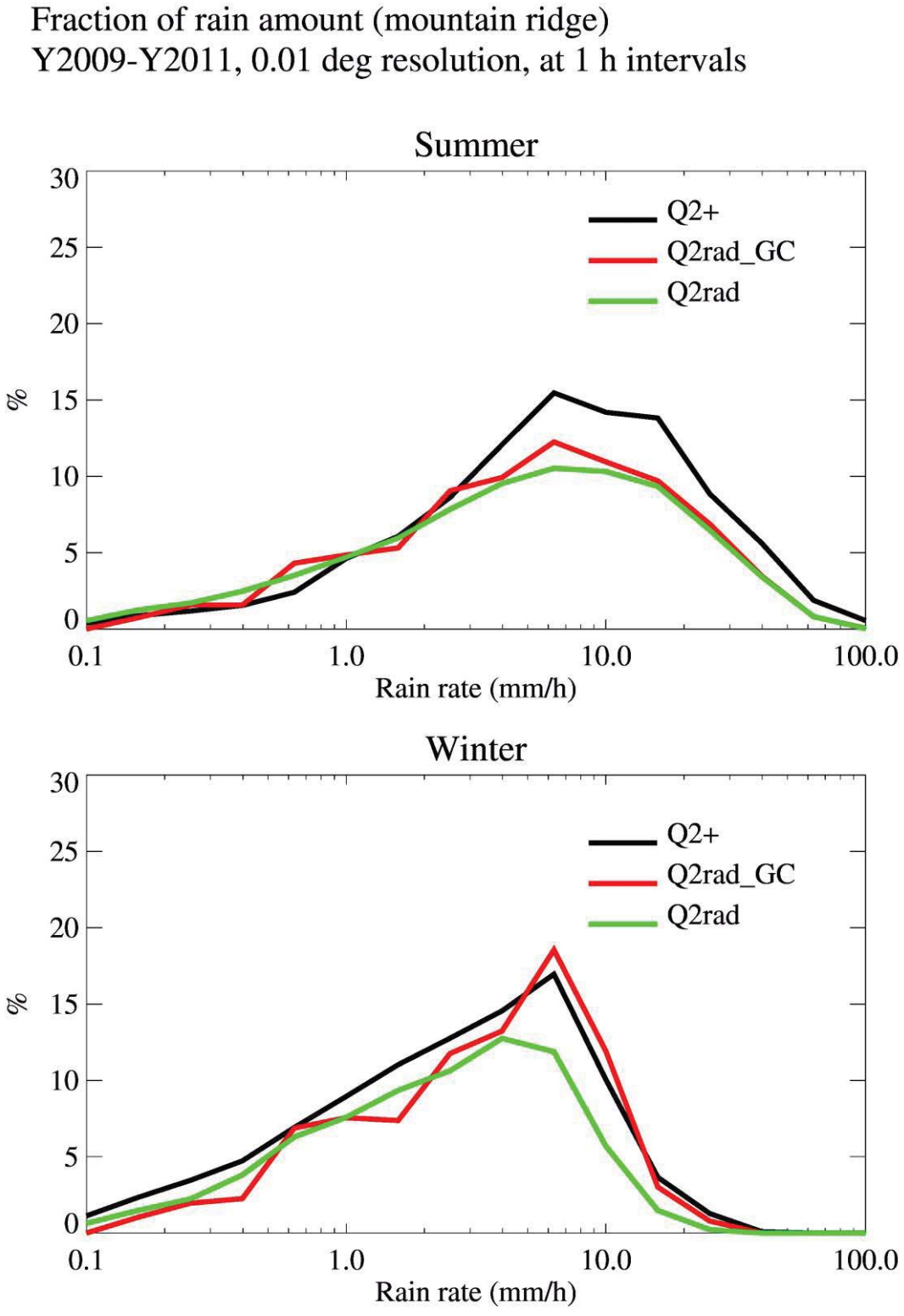

Figure 6: Fraction of rain amount as a function of rain intensity during summer (upper panel) and winter (lower panel) for rain events between 2009 and 2011 over mountain ridges.

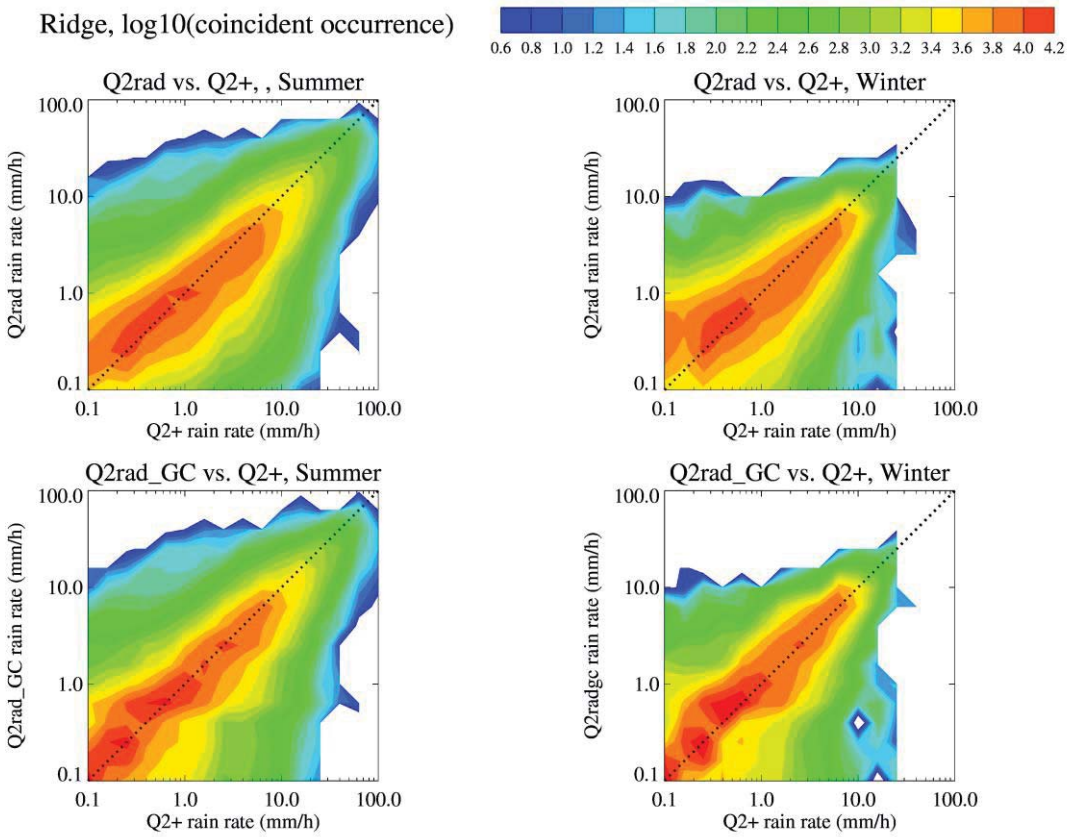

Figure 7: Joint distributions of coincident rain sample numbers during summer and winter over mountain ridges: between Q2+ and Q2rad (upper panels) and between Q2+ and Q2rad_GC (lower panels).

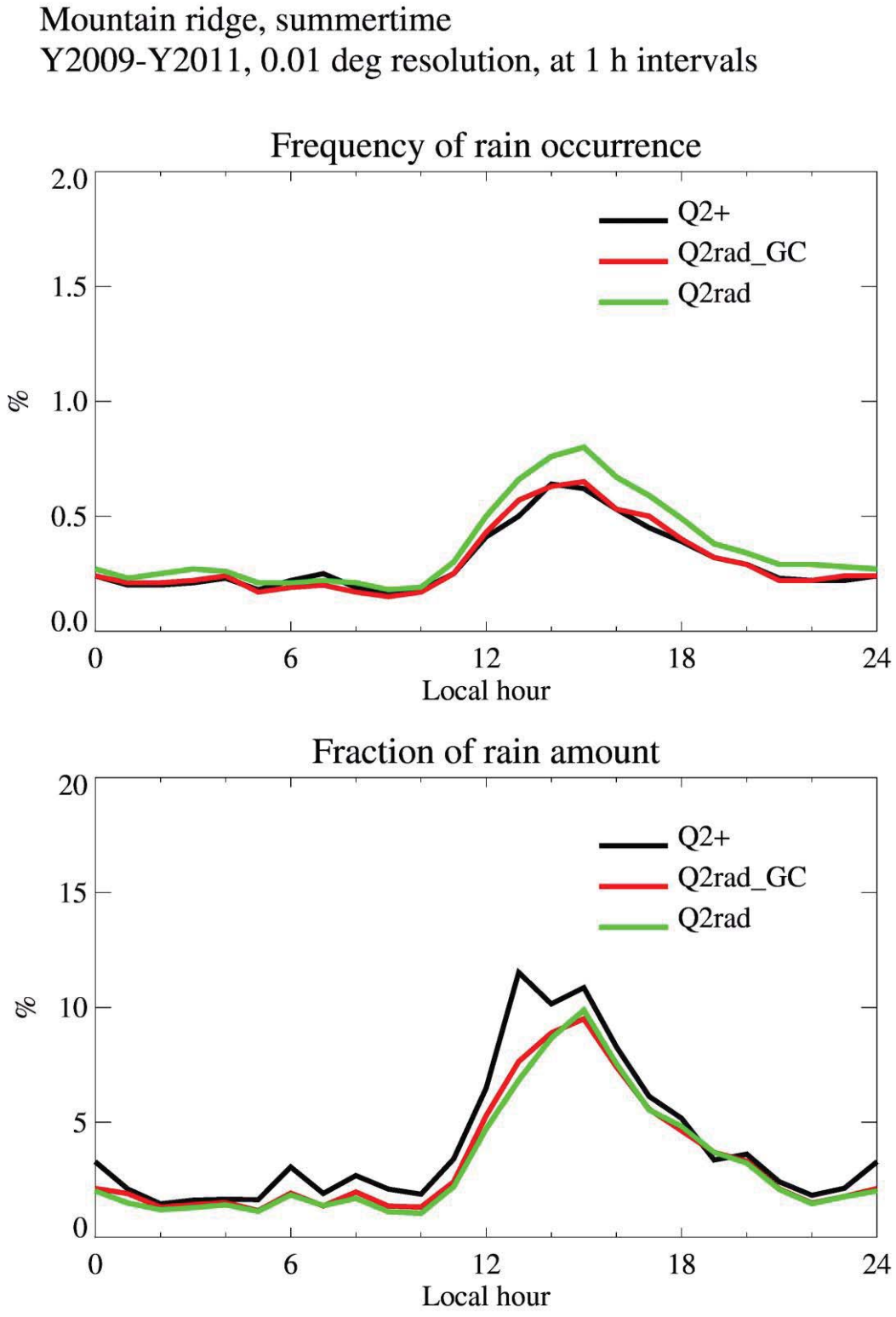

Figure 8: Diurnal variation of rain characteristics over mountain ridges during the summer. Upper panel: frequency of rain occurrence (%), lower panel: fraction of rain amount (%).

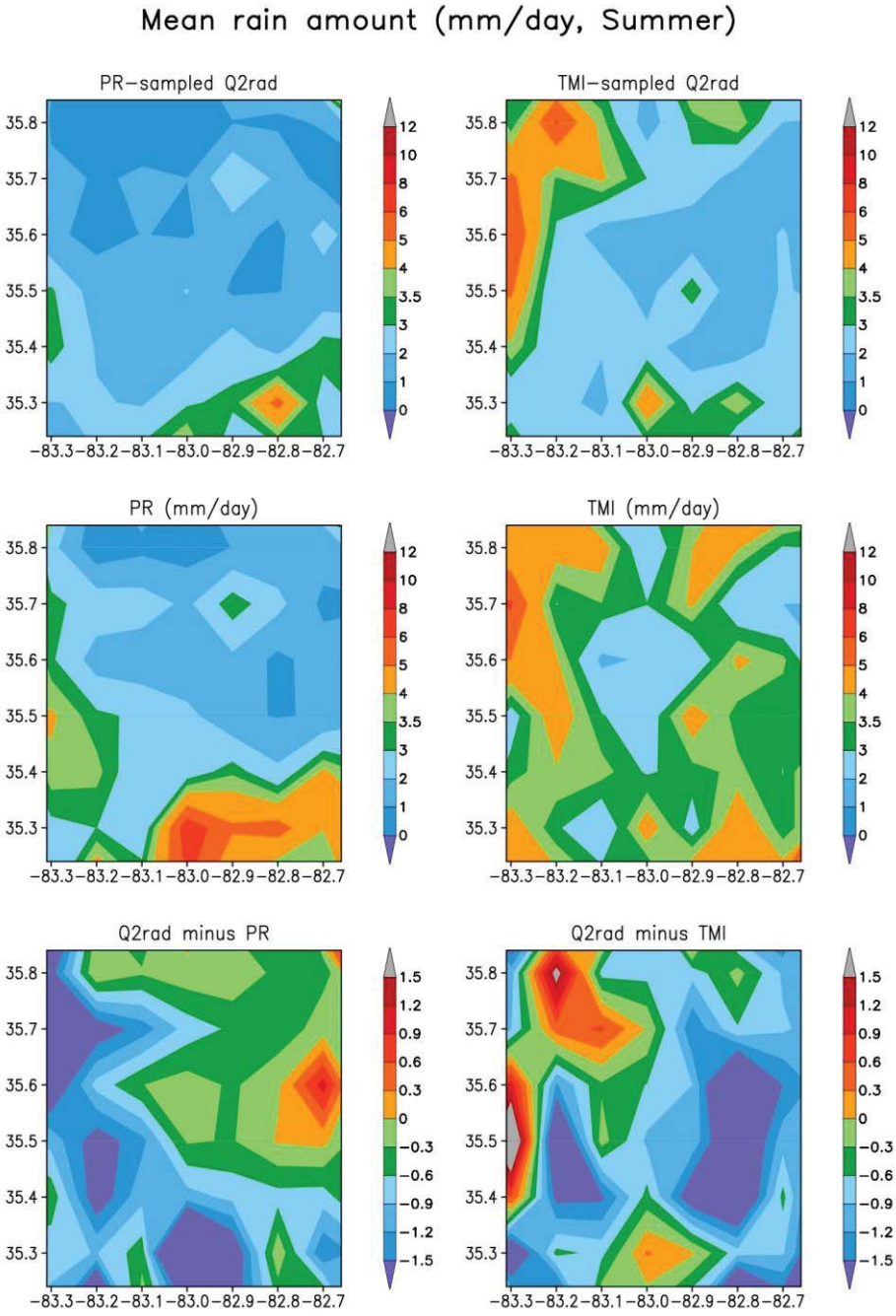

Figure 9: Mean rain amount from Q2rad, PR and TMI during the summer and the difference between surface radar rainfall and satellite rain retrievals.

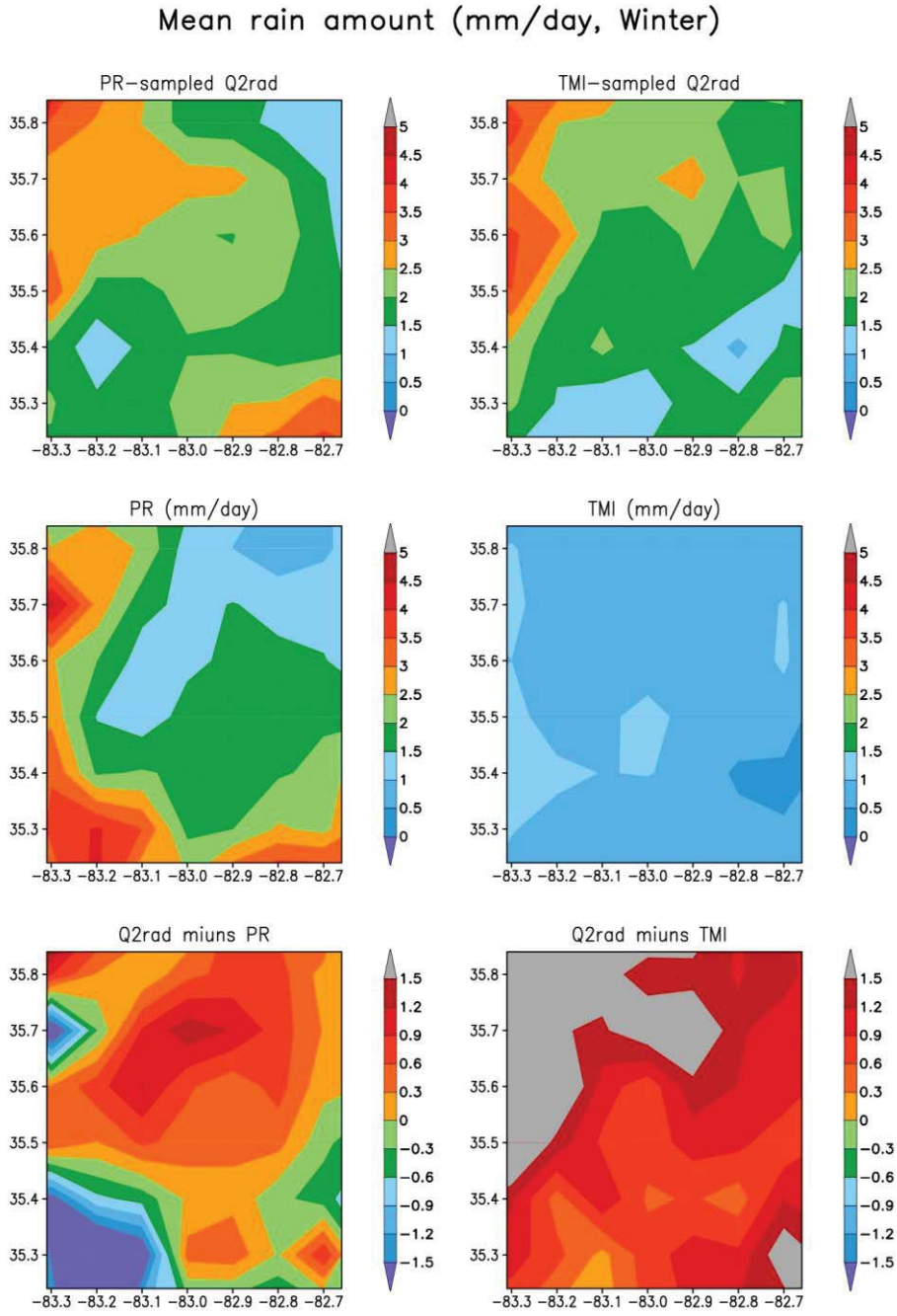

899
900 Figure 10: Mean rain amount from Q2rad, PR and TMI during the winter and the
901 difference between surface radar rainfall and satellite rain retrievals.
902
903
904

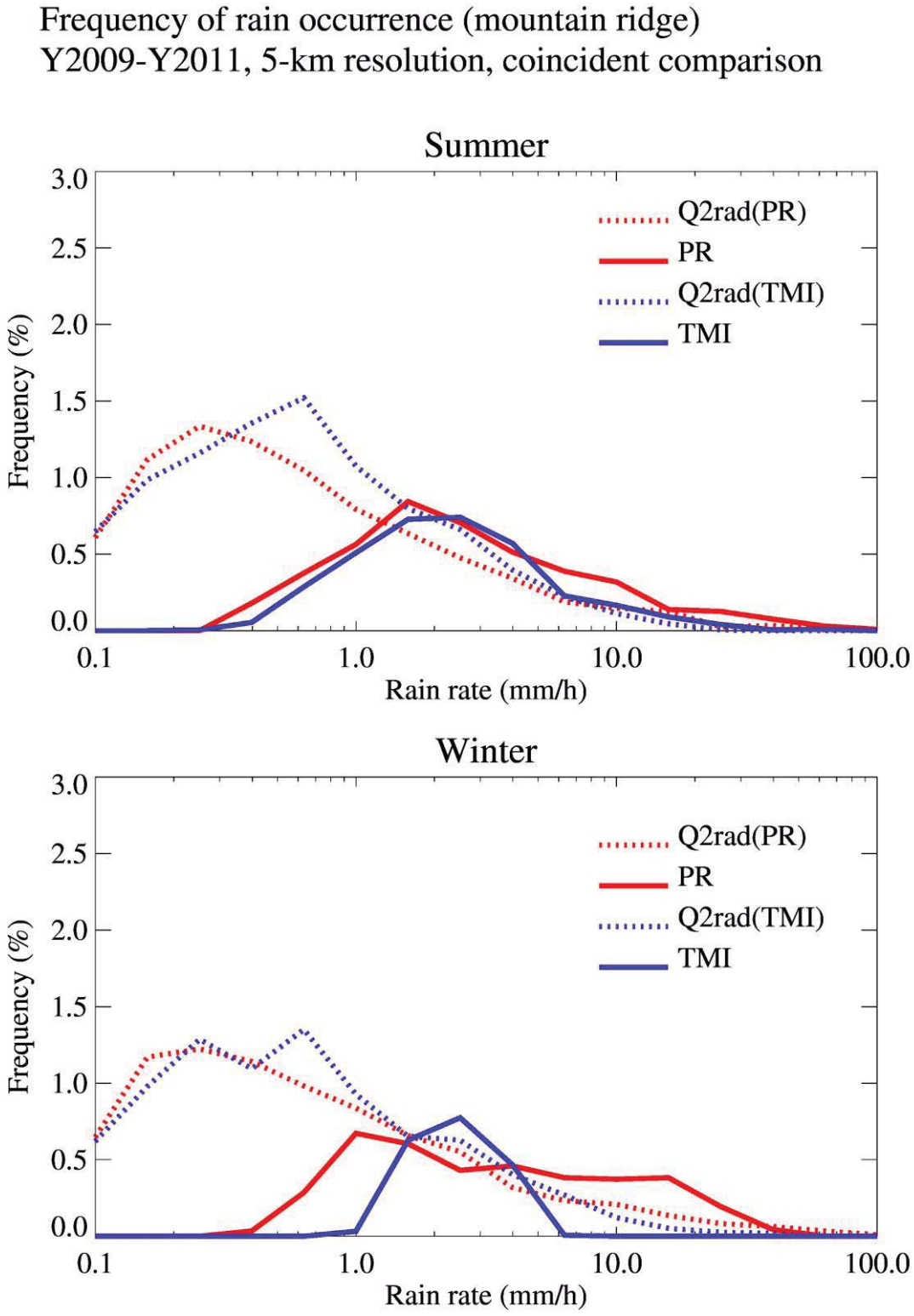

Figure 11: Frequency of rain occurrence (%) as a function of rain rate over mountain ridges during summer and winter for coincident rain samples of PR and PR-sampled Q2rad, and of TMI and TMI-sampled Q2rad.

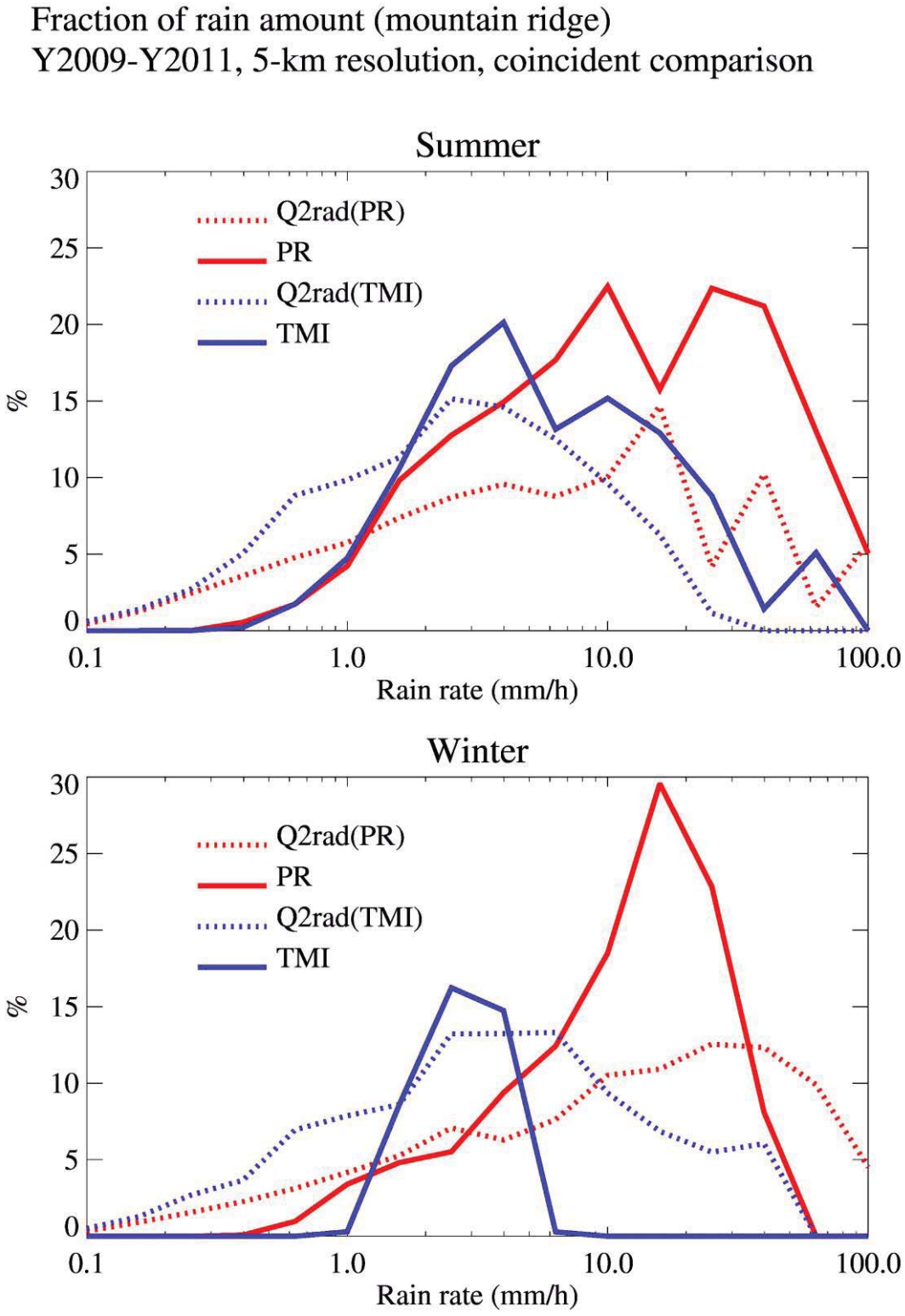

910
911 Figure 12: Same as Figure 11 but for fraction of rain amount over mountain ridges.
912

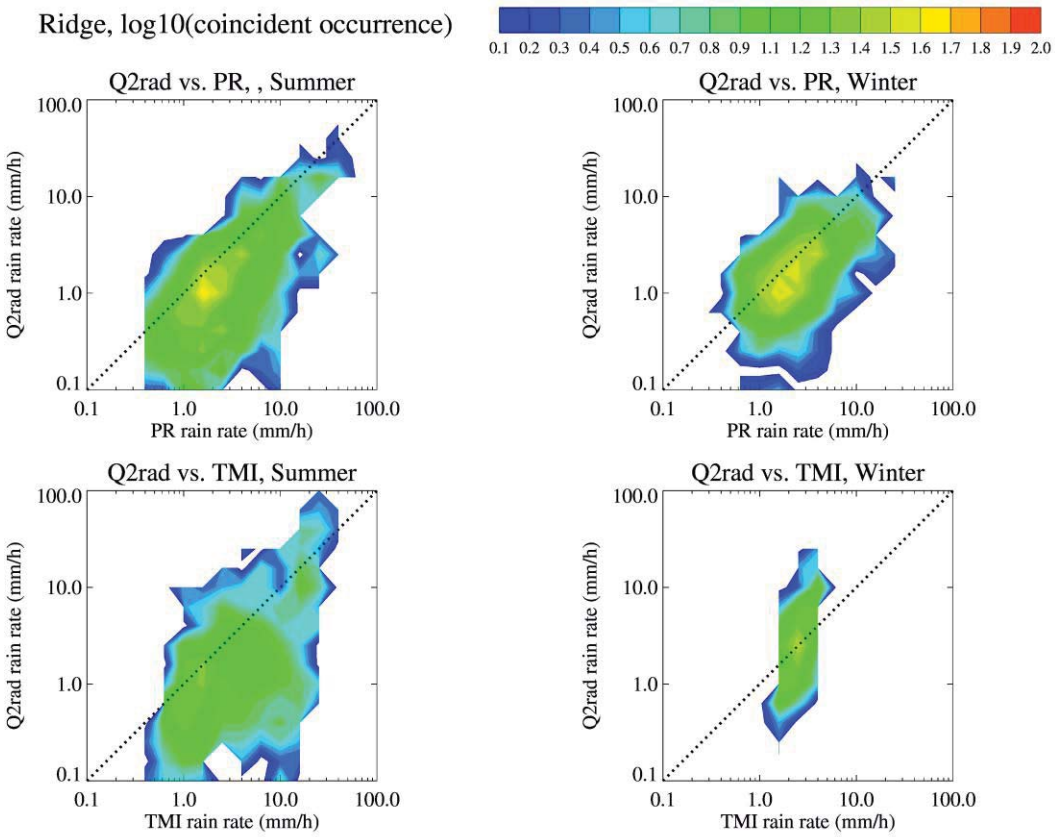

Figure 13: Joint distributions of coincident rain sample numbers during summer and winter over mountain ridges: between PR and Q2rad (upper panels) and between TMI and Q2rad (lower panels).